Research Article | Vol. 25, No. 22 | 30 Oct 2017 | OPTICS EXPRESS 26704
Optics EXPRESS

Magnetic Fano resonance of heterodimer nanostructure by azimuthally polarized excitation

Di Zhang, Jin Xiang, Hongfeng Liu, Fu Deng, Haiying Liu,* Min Ouyang, Haihua Fan, and Qiaofeng Dai

Guangdong Provincial Key Laboratory of Nanophotonic Functional Materials and Devices, School of Information and Optoelectronic Science and Engineering, South China Normal University, Guangzhou 510006, China
**hyliu@scnu.edu.cn*

Abstract: The optical properties of a Si-Au heterodimer nanostructure, which is composed of an Au split nanoring surrounded by a Si nanoring with a larger diameter, are investigated both theoretically and numerically. It is found that a pure magnetic plasmon Fano resonance can be achieved in the Si-Au heterodimer nanostructure when it is excited by an azimuthally polarized beam. It is revealed that the pure magnetic Fano resonance is generated by the destructive interference between the magnetic dipole resonance of the Si nanoring and the magnetic dipole resonance of the Au split nanoring. A coupled oscillator model is employed to analyze the Fano resonance of the Si-Au heterodimer nanostructure. The pure magnetic response of the Si-Au heterodimer nanostructure is verified by the current density distributions and the scattering powers of the electric and magnetic multipoles. The Fano resonance in the Si-Au heterodimer nanostructure exhibits potential applications of low-loss magnetic plasmon resonance in the construction of artificial magnetic metamaterials.

OCIS codes: (260.5740) Resonance; (250.5403) Plasmonics; (290.0290) Scattering.

References and links

1. J. Ye, F. Wen, H. Sobhani, J. B. Lassiter, P. Van Dorpe, P. Nordlander, and N. J. Halas, "Plasmonic nanoclusters: near field properties of the Fano resonance interrogated with SERS," Nano Lett. **12**(3), 1660–1667 (2012).
2. C. Wu, A. B. Khanikaev, and G. Shvets, "Broadband slow light metamaterial based on a double-continuum Fano resonance," Phys. Rev. Lett. **106**(10), 107403 (2011).
3. S. Zhang, K. Bao, N. J. Halas, H. Xu, and P. Nordlander, "Substrate-induced Fano resonances of a plasmonic nanocube: a route to increased-sensitivity localized surface plasmon resonance sensors revealed," Nano Lett. **11**(4), 1657–1663 (2011).
4. K. Lodewijks, J. Ryken, W. Van Roy, G. Borghs, L. Lagae, and P. Van Dorpe, "Tuning the Fano Resonance Between Localized and Propagating Surface Plasmon Resonances for Refractive Index Sensing Applications," Plasmonics **8**, 1379–1385 (2013).
5. W. S. Chang, J. B. Lassiter, P. Swanglap, H. Sobhani, S. Khatua, P. Nordlander, N. J. Halas, and S. Link, "A plasmonic Fano switch," Nano Lett. **12**(9), 4977–4982 (2012).
6. K. Nozaki, A. Shinya, S. Matsuo, T. Sato, E. Kuramochi, and M. Notomi, "Ultralow-energy and high-contrast all-optical switch involving Fano resonance based on coupled photonic crystal nanocavities," Opt. Express **21**(10), 11877–11888 (2013).
7. X. Liu, Y. Huo, M. Wang, S. Gao, C. Zhang, T. Ning, S. Jiang, P. Xiong, and B. Man, "A sensitive 2D plasmon ruler based on Fano resonance," RSC Advances **6**, 81757–81762 (2016).
8. A. E. Miroshnichenko, S. Flach, and Y. S. Kivshar, "Fano resonances in nanoscale structures," Rev. Mod. Phys. **82**, 2257–2298 (2010).
9. B. Luk'yanchuk, N. I. Zheludev, S. A. Maier, N. J. Halas, P. Nordlander, H. Giessen, and C. T. Chong, "The Fano resonance in plasmonic nanostructures and metamaterials," Nat. Mater. **9**(9), 707–715 (2010).
10. J. A. Fan, C. Wu, K. Bao, J. Bao, R. Bardhan, N. J. Halas, V. N. Manoharan, P. Nordlander, G. Shvets, and F. Capasso, "Self-assembled plasmonic nanoparticle clusters," Science **328**(5982), 1135–1138 (2010).
11. J. B. Lassiter, H. Sobhani, J. A. Fan, J. Kundu, F. Capasso, P. Nordlander, and N. J. Halas, "Fano resonances in plasmonic nanoclusters: geometrical and chemical tunability," Nano Lett. **10**(8), 3184–3189 (2010).

#302891 https://doi.org/10.1364/OE.25.026704
Journal © 2017 Received 24 Jul 2017; revised 7 Oct 2017; accepted 16 Oct 2017; published 18 Oct 2017

Optics EXPRESS

12. J. A. Fan, K. Bao, C. Wu, J. Bao, R. Bardhan, N. J. Halas, V. N. Manoharan, G. Shvets, P. Nordlander, and F. Capasso, "Fano-like interference in self-assembled plasmonic quadrumer clusters," Nano Lett. **10**(11), 4680–4685 (2010).
13. S.-D. Liu, Z. Yang, R.-P. Liu, and X.-Y. Li, "Multiple Fano Resonances in Plasmonic Heptamer Clusters Composed of Split Nanorings," ACS Nano **6**(7), 6260–6271 (2012).
14. S. H. Mousavi, I. Kholmanov, K. B. Alici, D. Purtseladze, N. Arju, K. Tatar, D. Y. Fozdar, J. W. Suk, Y. Hao, A. B. Khanikaev, R. S. Ruoff, and G. Shvets, "Inductive tuning of Fano-resonant metasurfaces using plasmonic response of graphene in the mid-infrared," Nano Lett. **13**(3), 1111–1117 (2013).
15. N. Verellen, Y. Sonnefraud, H. Sobhani, F. Hao, V. V. Moshchalkov, P. Van Dorpe, P. Nordlander, and S. A. Maier, "Fano resonances in individual coherent plasmonic nanocavities," Nano Lett. **9**(4), 1663–1667 (2009).
16. S. Zhang, D. A. Genov, Y. Wang, M. Liu, and X. Zhang, "Plasmon-induced transparency in metamaterials," Phys. Rev. Lett. **101**(4), 047401 (2008).
17. Y. H. Fu, J. B. Zhang, Y. F. Yu, and B. Luk'yanchuk, "Generating and manipulating higher order Fano resonances in dual-disk ring plasmonic nanostructures," ACS Nano **6**(6), 5130–5137 (2012).
18. J. Li, T. Liu, H. Zheng, J. Dong, E. He, W. Gao, Q. Han, C. Wang, and Y. Wu, "Higher Order Fano Resonances and Electric Field Enhancements in Disk-Ring Plasmonic Nanostructures with Double Symmetry Breaking," Plasmonics **9**, 1439–1445 (2014).
19. W. Liu, A. E. Miroshnichenko, D. N. Neshev, and Y. S. Kivshar, "Polarization-independent Fano resonances in arrays of core-shell nanoparticles," Phys. Rev. B **86**, 081407 (2012).
20. Z.-J. Yang, Q.-Q. Wang, and H.-Q. Lin, "Tunable two types of Fano resonances in metal–dielectric core–shell nanoparticle clusters," Appl. Phys. Lett. **103**, 111115 (2013).
21. P. Gu, M. Wan, W. Wu, Z. Chen, and Z. Wang, "Excitation and tuning of Fano-like cavity plasmon resonances in dielectric-metal core-shell resonators," Nanoscale **8**(19), 10358–10363 (2016).
22. W. Wu, M. Wan, P. Gu, Z. Chen, and Z. Wang, "Strong coupling between few molecular excitons and Fano-like cavity plasmon in two-layered dielectric-metal core-shell resonators," Opt. Express **25**(2), 1495–1504 (2017).
23. J. Wang, C. Fan, J. He, P. Ding, E. Liang, and Q. Xue, "Double Fano resonances due to interplay of electric and magnetic plasmon modes in planar plasmonic structure with high sensing sensitivity," Opt. Express **21**(2), 2236–2244 (2013).
24. Y. Li, Y. Huo, Y. Zhang, and Z. Zhang, "Generation and Manipulation of Multiple Magnetic Fano Resonances in Split Ring-Perfect Ring Nanostructure," Plasmonics **12**(5), 1613 (2016).
25. X. Ci, B. Wu, Y. Liu, G. Chen, E. Wu, and H. Zeng, "Magnetic-based Fano resonance of hybrid silicon-gold nanocavities in the near-infrared region," Opt. Express **22**(20), 23749–23758 (2014).
26. Y. Bao, Z. Hu, Z. Li, X. Zhu, and Z. Fang, "Magnetic plasmonic Fano resonance at optical frequency," Small **11**(18), 2177–2181 (2015).
27. A. E. Miroshnichenko and Y. S. Kivshar, "Fano resonances in all-dielectric oligomers," Nano Lett. **12**(12), 6459–6463 (2012).
28. B. Hopkins, D. S. Filonov, A. E. Miroshnichenko, F. Monticone, A. Alù, and Y. S. Kivshar, "Interplay of Magnetic Responses in All-Dielectric Oligomers To Realize Magnetic Fano Resonances," ACS Photonics **2**, 724–729 (2015).
29. B. Hopkins, W. Liu, A. E. Miroshnichenko, and Y. S. Kivshar, "Optically isotropic responses induced by discrete rotational symmetry of nanoparticle clusters," Nanoscale **5**(14), 6395–6403 (2013).
30. B. Hopkins, A. N. Poddubny, A. E. Miroshnichenko, and Y. S. Kivshar, "Revisiting the physics of Fano resonances for nanoparticle oligomers," Phys. Rev. A **88**, 053819 (2013).
31. D. S. Filonov, A. P. Slobozhanyuk, A. E. Krasnok, P. A. Belov, E. A. Nenasheva, B. Hopkins, A. E. Miroshnichenko, and Y. S. Kivshar, "Near-field mapping of Fano resonances in all-dielectric oligomers," Appl. Phys. Lett. **104**, 021104 (2014).
32. S. Lepeshov, A. Krasnok, I. Mukhin, D. Zuev, A. Gudovskikh, V. Milichko, P. Belov, and A. Miroshnichenko, "Fine-Tuning of the Magnetic Fano Resonance in Hybrid Oligomers via fs-Laser-Induced Reshaping," ACS Photonics **4**, 536–543 (2017).
33. K. E. Chong, B. Hopkins, I. Staude, A. E. Miroshnichenko, J. Dominguez, M. Decker, D. N. Neshev, I. Brener, and Y. S. Kivshar, "Observation of Fano resonances in all-dielectric nanoparticle oligomers," Small **10**(10), 1985–1990 (2014).
34. C. Guclu, M. Veysi, and F. Capolino, "Photoinduced Magnetic Nanoprobe Excited by an Azimuthally Polarized Vector Beam," ACS Photonics **3**, 2049–2058 (2016).
35. P. B. Johnson and R. W. Christy, "Optical Constants of the Noble Metals," Phys. Rev. B **6**, 4370–4379 (1972).
36. D. F. Edwards, "Silicon (Si)," in Handbook of Optical Constants of Solids, E. D. Palik, ed. (Academic, 1985).
37. T. Feng, Y. Xu, Z. Liang, and W. Zhang, "All-dielectric hollow nanodisk for tailoring magnetic dipole emission," Opt. Lett. **41**(21), 5011–5014 (2016).
38. S.-D. Liu, Z. Yang, R.-P. Liu, and X.-Y. Li, "High Sensitivity Localized Surface Plasmon Resonance Sensing Using a Double Split NanoRing Cavity," J. Phys. Chem. C **115**, 24469–24477 (2011).
39. E. Prodan, C. Radloff, N. J. Halas, and P. Nordlander, "A hybridization model for the plasmon response of complex nanostructures," Science **302**(5644), 419–422 (2003).
40. A. Lovera, B. Gallinet, P. Nordlander, and O. J. Martin, "Mechanisms of Fano resonances in coupled plasmonic systems," ACS Nano **7**(5), 4527–4536 (2013).

Optics EXPRESS

41. F. Xiao, W. Zhu, W. Shang, T. Mei, M. Premaratne, and J. Zhao, "Electrical control of second harmonic generation in a graphene-based plasmonic Fano structure," Opt. Express **23**(3), 3236–3244 (2015).
42. W. Shang, F. Xiao, W. Zhu, H. He, M. Premaratne, T. Mei, and J. Zhao, "Fano resonance with high local field enhancement under azimuthally polarized excitation," Sci. Rep. **7**(1), 1049 (2017).
43. T. Kaelberer, V. A. Fedotov, N. Papasimakis, D. P. Tsai, and N. I. Zheludev, "Toroidal dipolar response in a metamaterial," Science **330**(6010), 1510–1512 (2010).
44. W. Liu, J. Zhang, and A. E. Miroshnichenko, "Toroidal dipole-induced transparency in core-shell nanoparticles," Laser Photonics Rev. **9**, 564–570 (2015).
45. T. Feng, Y. Xu, W. Zhang, and A. E. Miroshnichenko, "Ideal Magnetic Dipole Scattering," Phys. Rev. Lett. **118**(17), 173901 (2017).
46. K. Aydin, I. M. Pryce, and H. A. Atwater, "Symmetry breaking and strong coupling in planar optical metamaterials," Opt. Express **18**(13), 13407–13417 (2010).
47. M. Najiminaini, F. Vasefi, B. Kaminska, and J. J. L. Carson, "Nano-hole array structure with improved surface plasmon energy matching characteristics," Appl. Phys. Lett. **100**, 043105 (2012).

1. Introduction

Fano resonance based on artificial plasmon structure has become the focus of research in recent years for its wide applications in the areas such as surface enhanced Raman scattering (SERS) [1], slow-light devices [2], biological and chemical sensors [3,4], optical switch [5,6], and plasmon ruler [7]. Fano resonance, exhibiting an asymmetric line shape and inducing a large electromagnetic field enhancement [8,9], results from the interactions of narrow subradiant modes and broad superradiant modes. So far, numerous nanostructures have been designed to generate Fano resonance, such as nanoparticle clusters [10–13], dolmen structures [14–16], nonconcentric ring/disk cavities [17,18], core-shell structures [19–22].

Due to the deficiency of natural magnetism in metal nanomaterials at optical frequencies, the initial Fano resonance was studied mainly based on the pure electric responses in metal nanostructures. And then researchers began to focus on magnetic-based Fano resonance due to its potential application of artificial magnetism. The magnetic-based Fano resonance had been studied in many plasmonic structures. Wang et al. demonstrated that the double Fano resonance effect can be achieved in the SRRs/Rod structure due to the interplay of electric and magnetic plasmon modes [23]. Li et al. observed multiple magnetic Fano resonance in split ring-perfect ring nanostructure [24]. Ci et al. theoretically demonstrated a magnetic-based Fano resonance of hybrid silicon-gold nanocavities in the near-infrared region [25]. The magnetic-based Fano resonance generally originates from the coupling between the electric dipole resonance mode and the magnetic dipole resonance mode. However, the dominant scattering from the electric dipole leads to a high radiative loss, which limits its application area. Therefore, the research on the pure magnetic plasmon Fano resonance have become a popular topic. Bao et al. demonstrated that a pure magnetic plasmon Fano resonance can be realized at optical frequency with Au split ring hexamer nanostructure [26]. Miroshnichenko et al. theoretically and experimentally demonstrated that the magnetic Fano resonances can be achieved in the nanoparticle oligomer structures due to the interplay of magnetic responses [27–33].

In this paper, we investigated the optical properties of a Si-Au heterodimer nanostructure (Si-Au HDNS), which is composed of an Au split nanoring (Au SNR) surrounded by a Si nanoring (Si NR) with a larger diameter. An azimuthally polarized beam (APB) is utilized as the incident light source. At each point, the electric field of the APB is linearly polarized but its vector is oriented perpendicularly to the radius vector from the beam axis. In most studies, a plane wave or a focused Gaussian beam was generally used as the incident light source, which was either linearly or circularly polarized. Recently, it was shown that the APB has the capability to effectively excite the magnetic dipole resonance and suppress the electric dipole resonance of the nanostructure [34]. In this way, the magnetic dipole resonances of the Si NR and Au SNR can be excited effectively, resulting in the generation of the pure magnetic plasmon Fano resonance. We have demonstrated that a pure magnetic Fano resonance can be achieved in a Si-Au HDNS excited by an APB. It is shown that the pure magnetic Fano resonance originates from the interaction between the magnetic dipole resonance of the Si NR

Optics EXPRESS

and the magnetic dipole resonance of the Au SNR. These two interacting modes could be regarded as two coupled oscillators, a coupled oscillator model is employed to analyze the Fano resonance of the Si-Au heterodimer nanostructure. The wavelength as well as intensity of the Fano resonance can be adjusted effectively by tuning the geometry parameters of the Si–Au HDNS. Due to the interplay of the two magnetic modes, magnetic hybridization with reduced radiative loss can be realized, which could be beneficial to the development of low loss plasmonic applications such as low-loss sensors.

2. Structures and simulation method

The three-dimensional and two-dimensional schematic diagrams of the Si-Au HDNS are shown in Figs. 1(a) and 1(b), respectively. The inner and outer radius of the Au SNR is r_1 and r_2, located at the center of the Si NR with the inner radius r_3, outer radius r_4. The thickness of the Si NR and the Au SNR are both T, and the gap length of Au SNR is g. The dielectric constants of gold and silicon are taken from Refs [35] and [36], respectively.

The numerical simulations are performed by the finite difference time domain (FDTD) Solutions software. The APB source is utilized as the incident light propagating in z direction, at each point, the electric field of the APB is linearly polarized but its vector is oriented perpendicularly to the radius vector from the beam axis. Figure 1(c) shows the intensity and electric vector distributions of the APB. To avoid the interference of the reflection from the boundaries, we set perfect match layers (PML) outside the nanostructure to absorb all electromagnetic waves inside the PML. The refractive index of the surrounding is 1.

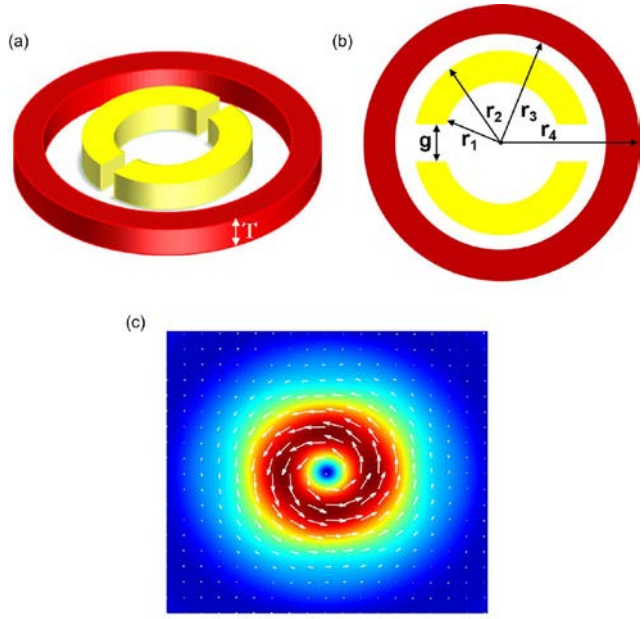

Fig. 1. (a) Three-dimensional and (b) two-dimensional schematic diagrams for the Si-Au HDNS with the descriptions of the geometrical parameters. (c) Intensity and electric vector distributions of the APB.

Optics EXPRESS

3. Results and discussion

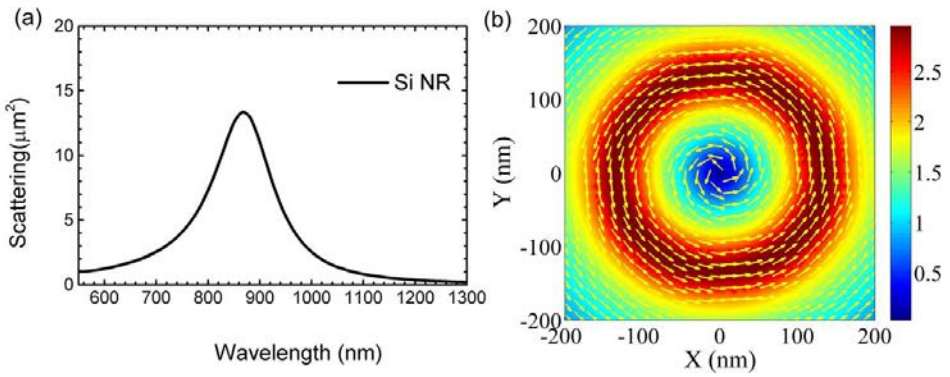

Fig. 2. (a) Scattering spectra of the Si NR with the illumination of the APB. (b) The field enhancement and current density distributions of the Si NR at 868nm.

First of all, the optical properties of the Si NR and the Au SNR are investigated. In consideration of plasmon coupling intensity, the parameters of the Si-Au HDNS are set as: r_1 = 45 nm, r_2 = 85 nm, r_3 = 110 nm, r_4 = 160 nm, g = 35 nm and T = 100 nm. An APB source is utilized as the incident light propagating in z direction. It is shown that the magnetic dipole could be excited effectively in both of the Si NR and Au SNR. As shown in Fig. 2, for the Si NR, only the magnetic dipole mode centered at 868 nm can be excited by the APB. The magnetic dipole mode is characterized by circular displacement currents on the Si NR, which is similar to that described for a silicon hollow nanodisk [37]. For the Au SNR, as shown in Fig. 3, there is a sole resonance peak at 874 nm, corresponding to the magnetic dipole mode, which is characterized by induced antisymmetric circular displacement currents on the two half rings. This induced magnetic mode couples weakly to the external optical field and could not be excited directly under a linearly polarized beam at normal incidence [38], but it could be efficiently excited by the APB.

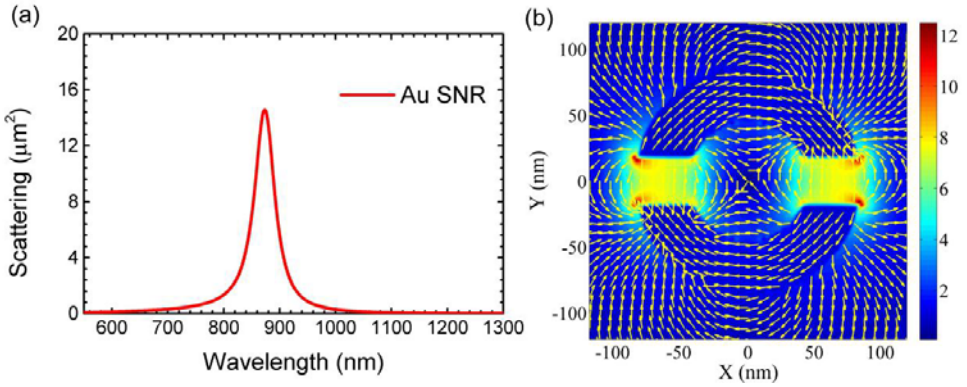

Fig. 3. (a) Scattering spectra of the Au SNR with the illumination of the APB. (b) The field enhancement and current density distributions of the Au SNR at 874 nm.

We also calculated the scattering spectra of the Si-Au HDNS excited by the APB in order to better understand its optical properties. When the Si NR and Au SNR are aligned together to form a heterodimer nanostructure, one can see that a representative Fano resonance spectral response with its dip at 842 nm and peaks at 759 and 996 nm respectively appears in Fig. 4(a). The Fano resonance results from the interaction between a narrow magnetic mode and a broad magnetic mode. The field enhancement and current density distributions of the resonance dip are presented in Fig. 4(c), and the field enhancement and current density

Optics EXPRESS

distributions of the resonance peaks are presented in Figs. 4(b) and 4(d), respectively. From the viewpoint of plasmon hybridization theory, the coupling between the two plasmon modes results in splitting of the modal energies into bonding and anti-bonding resonances [39]. One can see that the resonance with a higher energy around 759 nm is the anti-bonding dipole-dipole mode, and the resonance with a lower energy around 996 nm is the bonding dipole-dipole mode. It can be found that the field enhancement is mainly concentrated in the gap of the Au SNR and the space between the Si NR and Au SNR, which represents the strong coupling between the Si NR and Au SNR. It is demonstrated that Fano resonance derives from the interaction of magnetic dipole modes, judging from their current density distributions.

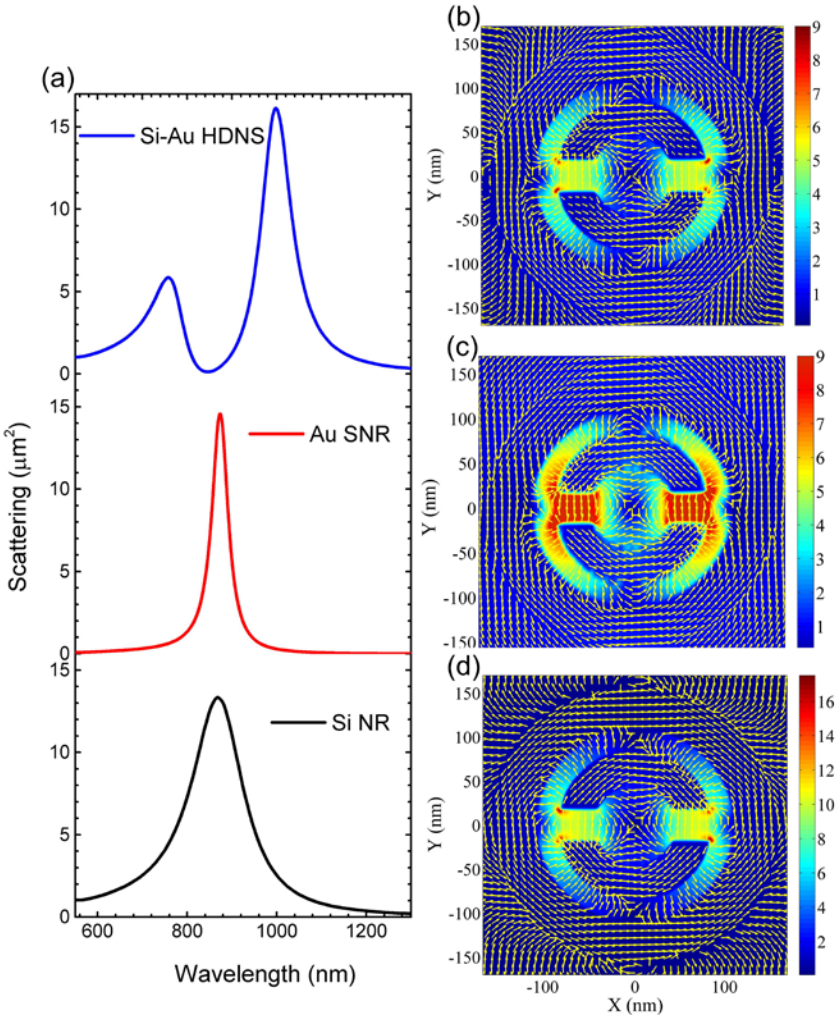

Fig. 4. (a) Scattering spectra (left panel) of the Si NR (bottom), Au SNR (middle) and Si-Au HDNS (top) with the illumination of the APB. (b) and (d) show the field enhancement and current density distributions (right panel) of the resonance peaks. (c) shows the field enhancement and current density distributions (right panel) of the resonance dip.

The Fano resonance of the Si-Au HDNS excited by the APB can be interpreted as the interference between a broad magnetic mode and a narrow magnetic mode. These two interacting modes could be regarded as two coupled oscillators, the two oscillators provide

Optics EXPRESS

the bonding mode and anti-bonding mode. The equation governing the motions of the two oscillators can be written as [40–42]:

$$\begin{aligned}\frac{d^2x_a}{dt^2}+\gamma_a\frac{dx_a}{dt}+\omega_a^2x_a+gx_b&=\frac{1}{2}\left(\eta_b\frac{d^3x_b}{dt^3}+\eta_a\frac{d^3x_a}{dt^3}\right)+\eta_aE\\ \frac{d^2x_b}{dt^2}+\gamma_b\frac{dx_b}{dt}+\omega_b^2x_b+gx_a&=\frac{1}{2}\left(\eta_b\frac{d^3x_b}{dt^3}+\eta_a\frac{d^3x_a}{dt^3}\right)+\eta_bE\end{aligned} \tag{1}$$

where $\omega_{a(b)}$, $\gamma_{a(b)}$ and $\eta_{a(b)}$ are the resonance frequency, nonradiative damping and radiation coupling efficiency of the anti-bonding (bonding) mode, respectively. g represents the coupling constant between the two oscillators and E denotes as $E = E_0e^{i\omega t}$ is the electrical field of the excitation beam. The motions of two oscillators are harmonics with forms of $x_{a(b)} = C_{a(b)}e^{i\omega t}$, where $C_{a(b)}(\omega)$ can be analytically derived

$$C_a(\omega)=\frac{\left(g+\frac{i}{2}\eta_b\omega^3\right)C_b(\omega)-\eta_aE_0}{\omega^2-i\gamma_a\omega-\omega_a^2-\frac{i}{2}\eta_a\omega^3}$$

$$C_b(\omega)=\frac{-\eta_aE_0\left(g+\frac{i}{2}\eta_a\omega^3\right)-\eta_bE_0\left(\omega^2-i\gamma_a\omega-\omega_a^2-\frac{i}{2}\eta_a\omega^3\right)}{\left(\omega^2-i\gamma_a\omega-\omega_b^2-\frac{i}{2}\eta_b\omega^3\right)\left(\omega^2-i\gamma_a\omega-\omega_a^2-\frac{i}{2}\eta_a\omega^3\right)-\left(g+\frac{i}{2}\eta_b\omega^3\right)\left(g+\frac{i}{2}\eta_a\omega^3\right)} \tag{2}$$

These values can be utilized to calculate $\sigma_{sca}=I_0+\left|C_a+C_b\right|^2$ with I_0 accounting for the background, which is used to describe the scattering spectrum of the Si-Au HDNS. As shown in Fig. 5, a good agreement between the theory (red solid curves) and simulation (blue dots) is achieved.

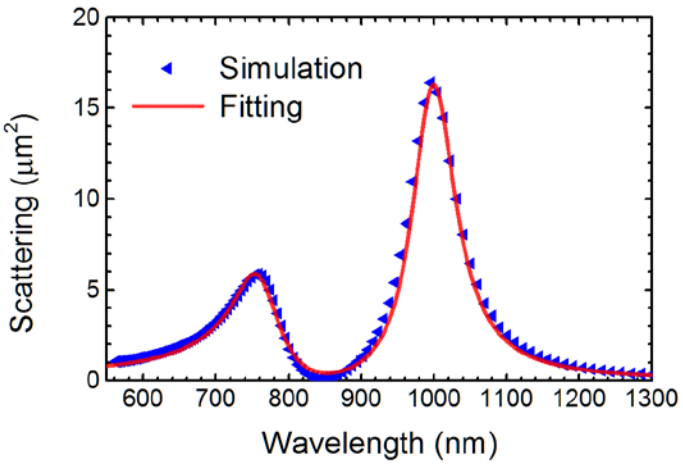

Fig. 5. Scattering spectra of the Si-Au HDNS excited by the APB, where the blue dots and red solid curves are the simulation and fitting results, respectively.

In order to further testify the optical scattering is dominated by the magnetic response, simulated densities of induced electrical currents were used to calculate scattered powers of the electric and magnetic multipoles, which are represented as [43]:

Optics EXPRESS

$$I = \frac{2\omega^4}{3c^3}|\mathrm{p}|^2 + \frac{2\omega^4}{3c^3}|\mathrm{m}|^2 + \frac{\omega^6}{5c^5}\sum|\mathrm{Q}_{\alpha\beta}|^2 + \frac{\omega^6}{20c^5}\sum|\mathrm{M}_{\alpha\beta}|^2 \quad (3)$$

where c is the speed of light, ω is the frequency of light and α, β = x, y, z. And the first and second terms originate from the electric and magnetic dipole scattering. The third and fourth terms correspond to the electric and magnetic quadrupole scattering. In the multipole expansion, the polarization current $J_P = \partial P/\partial t$ was used as the induced volume current j, which had the form $-i\omega P = -i\omega\varepsilon_0(\varepsilon_r-1)E$ in the case of harmonic excitation ~exp(-iωt). Based on the current distribution, the electric dipole (p), magnetic dipole (m), electric quadrupole ($Q_{\alpha\beta}$), and magnetic quadrupole ($M_{\alpha\beta}$) can be expressed on a Cartesian basis (α, β = x, y, z) as follows [44,45]:

$$\mathrm{p} = \frac{1}{-i\omega}\int \mathrm{j}\,d^3r \quad (4)$$

$$\mathrm{m} = \frac{1}{2c} = \int(\mathrm{r}\times\mathrm{j})d^3r \quad (5)$$

$$\mathrm{Q}_{\alpha\beta} = \frac{1}{-2i\omega} = \int\left[r_\alpha j_\beta + r_\beta j_\alpha - \frac{2}{3}(r\cdot j)\delta_{\alpha\beta}\right]d^3r \quad (6)$$

$$\mathrm{M}_{\alpha\beta} = \frac{1}{3c}\int\left[(\mathrm{r}\times\mathrm{j})_\alpha r_\beta + (\mathrm{r}\times\mathrm{j})_\beta r_\alpha\right]d^3r \quad (7)$$

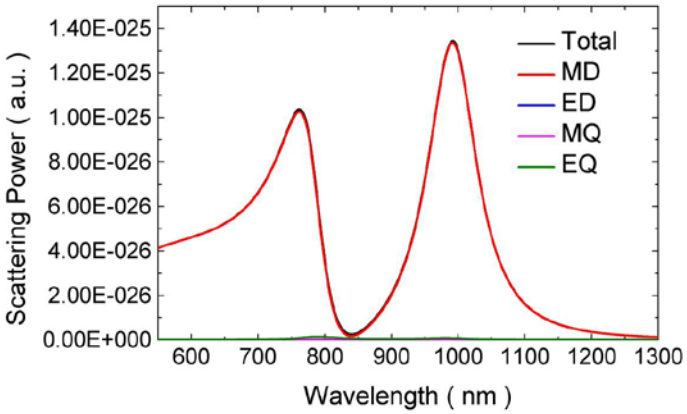

Fig. 6. Scattering power of the multipoles as a function of the wavelength, the contributions of the magnetic dipole (MD), electric dipole (ED), magnetic quadrupole (MQ), and electric quadrupole (EQ) to the total scattering are revealed.

Figure 6 shows the scattering powers of the multipoles in the Si-Au HDNS, which reveals the contributions of the magnetic dipole (MD), electric dipole (ED), magnetic quadrupole (MQ), and electric quadrupole (EQ) to the total scattering. It is demonstrated that magnetic dipole scattering dominates the total scattering, validating the pure magnetic response of the Si-Au HDNS.

Optics EXPRESS

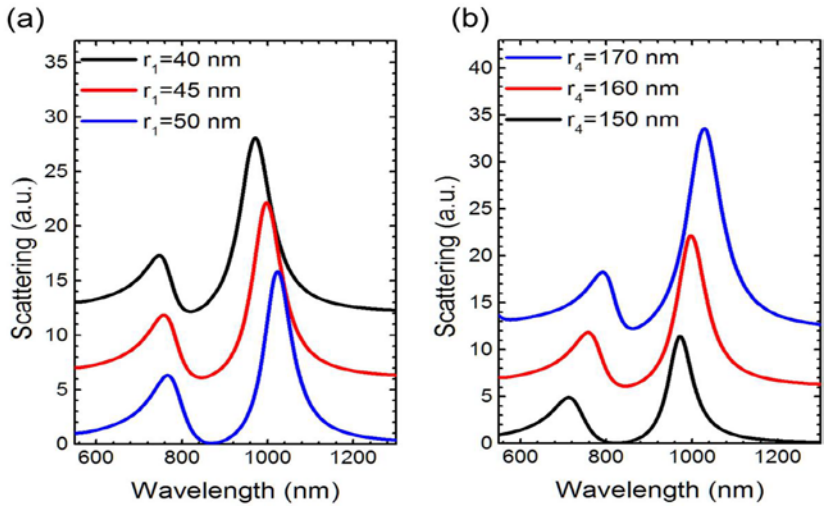

Fig. 7. Scattering cross sections of the Si-Au HDNS with (a) different Au SNR inner radius r_1 and (b) different Si NR outer radius r_4.

In order to get insight into the origins of the resonances, we further investigate the effects of the outer radius of the Si NR (r_4), the inner radius of the Au SNR (r_1), the gap length of the Au SNR (g), and the thickness of the rings (T) on the spectra position and intensity of the Fano resonances. In Fig. 7, we investigate the resonance wavelength and intensity of the magnetic Fano resonance by varying the inner radius of the Au SNR (r_1) and the outer radius of the Si NR (r_4). With the increasing of r_1 and r_4, the scattering spectra of Fano resonance are red shifted obviously.

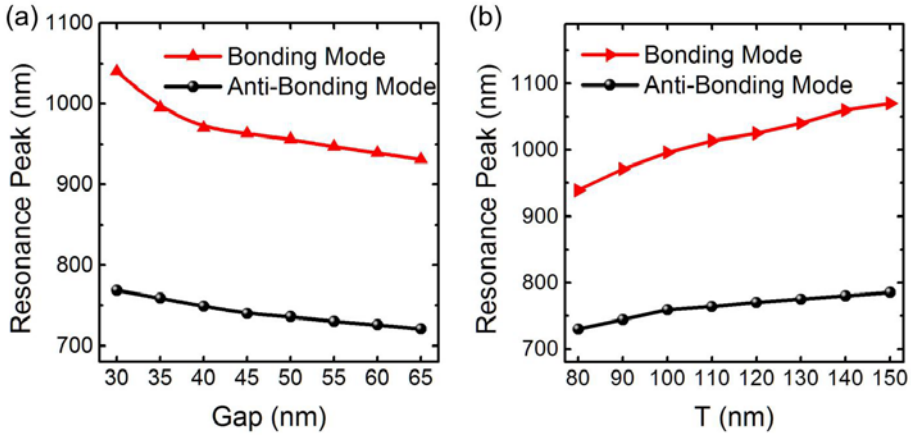

Fig. 8. The resonance peak wavelengths of the bonding mode and anti-bonding mode versus (a) the gap length of the Au SNR and (b) the thickness of the rings

The relationships between the resonance peak wavelengths of the two coupling modes and the gap length of the Au SNR are shown in Fig. 8(a). One can see that the two coupling modes are blue shifted with the increasing of gap length (g). According to LC circuit resonance model, in U-shaped split ring resonator (SRR), the resonance wavelength is proportional to $(LC)^{1/2}$, where L is the inductance of SRR and C is the capacitance between the two arms which is inversely proportional to the gap length [46]. This explains the phenomenon that resonances exhibit an obvious blueshift with increasing of gap length. In Fig. 8(b), we investigate the resonance peak shift of the bonding mode and anti-bonding mode

Optics EXPRESS

with increasing of thickness of the rings. It should be noted that the thickness of the Si NR and Au SNR is changed simultaneously. As shown in Fig. 8(b), the two coupling modes are red shifted when increasing thickness (T) from 80 nm to 150 nm.

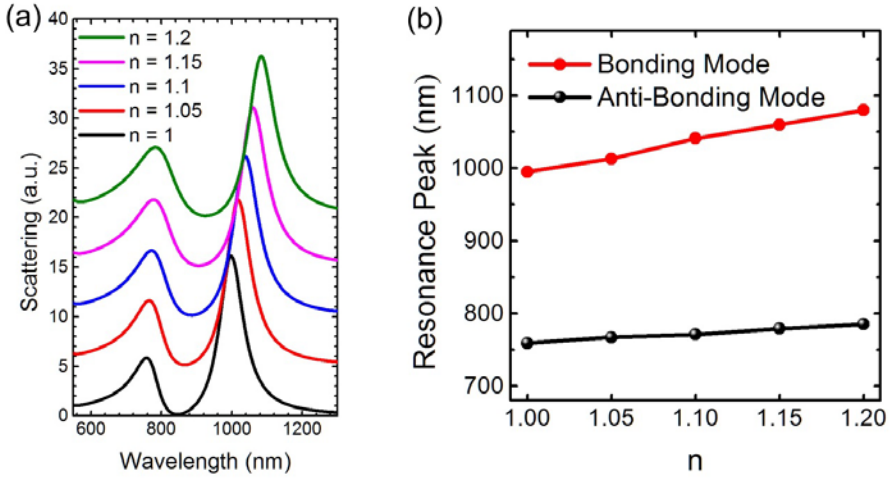

Fig. 9. (a) Scattering cross sections of the Si-Au HDNS as a function of the refractive index of the environment. (b) The resonance peak wavelengths of the bonding mode and anti-bonding mode versus the refractive index of the environment.

In order to investigate the sensing performance of the Si-Au HDNS, the scattering spectra with different dielectric environments are shown in Fig. 9(a). Figure 9(b) shows the resonance peak wavelengths of the bonding mode and anti-bonding mode vs. environmental refractive index. The two modes exhibit a red shift with increasing of refractive index. This can be understood by the fact that the resonance wavelength is proportional to the refractive index of the media environment [47]. The sensitivity (resonance peak shift per index refractive of external medium) and figure of merit (FOM = $(\delta\lambda/\delta n)$/linewidth) were used to describe the spectral shift of resonances and the sensing performance [38]. In order to investigate the sensing performance, the sensitivity and figure of merit are investigated. The sensitivity (450 nm/RIU) and figure of merit (FOM = 6.1) can be obtained at bonding mode, and therefore our low-loss magnetic Fano resonance can be used as a basis for the sensor applications.

4. Conclusion

In summary, we have demonstrated that a pure magnetic Fano resonance can be achieved in a Si-Au HDNS excited by an APB. In this way, the magnetic dipole resonances of the Si NR and Au SNR can be excited effectively, leading to the formation of the pure magnetic plasmon Fano resonance. The wavelength and intensity of the Fano resonance can be adjusted by varying the geometry parameters of the Si–Au HDNS. The tunable magnetic Fano resonance proposed in this work may find potential applications in novel photonic devices such as low-loss sensors.

Funding

National Natural Science Foundation of China (Grant No. 61201102, 11204092); Natural Science Foundation of Guangdong Province, China (Grant. No. S201204000634, 2016A030313851).

Acknowledgments

The anthors acknowledge Professor Sheng Lan for his guidance.